APPLICATION OF AMSU FOR OBTAINING WATER VAPOR, CLOUD LIQUID WATER, PRECIPITATION, SNOW COVER AND SEA ICE CONCENTRATION

Norman Grody, Fuzhong Weng and Ralph Ferraro NOAA/NESDIS/Office of Research and Applications 5200 Auth Road, Room 601 Camp Springs, MD USA 20746

1. INTRODUCTION

Microwave instruments are used to probe through the Earth's cloud cover and measure the underlying surface and atmospheric parameters. As shown in Figure 1, they were first flown aboard U.S. satellites in 1972. At that time the National Aeronautic and Space Administration (NASA) first began flying microwave radiometers aboard the Nimbus series of satellites. The first radiometers were flown on Nimbus-E, but had few channels with poor spatial coverage. These initial sensors were soon replaced by more advanced instruments until the Nimbus program ended in 1978 with the launch of the Scanning Multichannel Microwave Radiometer (SMMR) on Nimbus-G. Measurements from these experimental units were used to advance our knowledge of instrument design and improve the use of microwaves for observing the Earth from space.

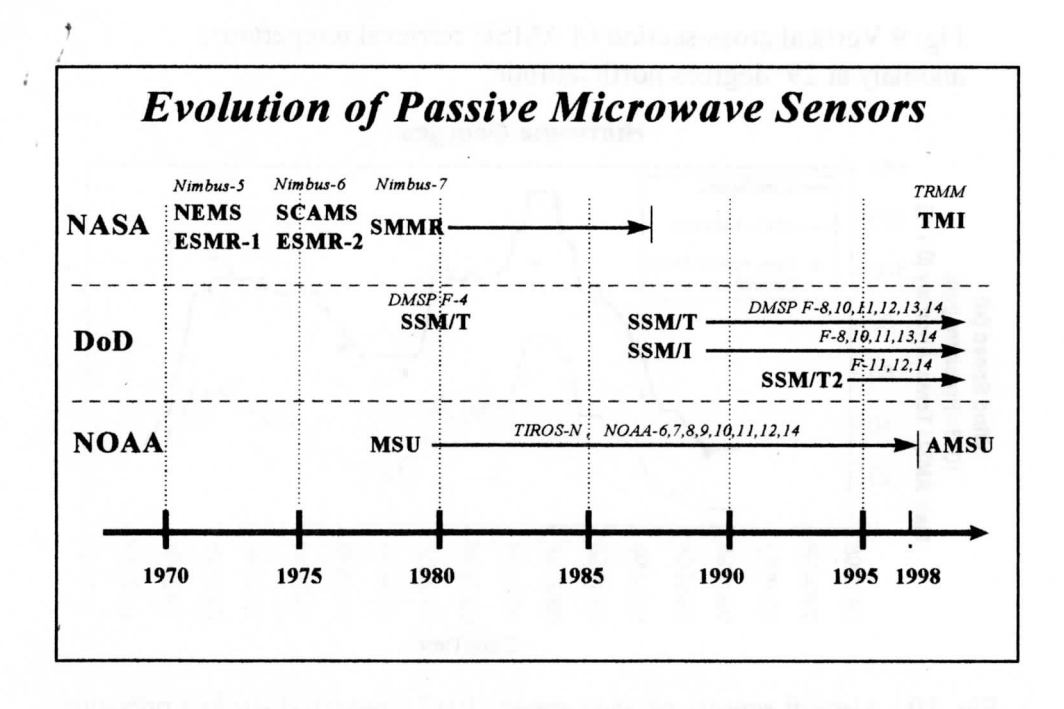


Figure 1. Chronology of microwave sensor development

Beginning in 1978, the National Oceanic and Atmospheric Administration (NOAA) launched its first microwave radiometer, called the Microwave Sounding Unit (MSU), aboard the TIROS series of polar orbiting satellites (see Fig. 1). This operational instrument was designed similar to the Scanning Microwave Spectrometer (SCAMS), which was flown on Nimbus-F in 1973. The MSU contains four channels in the 50 to 60 GHz portion of the oxygen band to derive temperature soundings from the surface to about 50 mb. A number of identical instruments have been flown over the past twenty years, each having exceptionally high stability and precision. The high performance of the MSU instruments have made it possible to monitor very small climatic changes in temperature, with an accuracy less than 0.1 K (Spencer et al., 1990).

During the past ten years there has been a dramatic increase in the use of microwave derived products by the world-wide community of meteorological and oceanographic organizations. This greater emphasis is primarily attributed to the launch of the Special Sensor Microwave Imager (SSM/I) in 1987 onboard the first of a series of DMSP (Defense Meteorological Satellite Program) satellites (see Fig. 1). In contrast to temperature sounders, the microwave imager contains six channels in window regions (19, 37, 85 GHz) with dual polarization, and a seventh channel centered on the 22.23 GHz water vapor line with vertical polarization. Products such as rainfall, snow cover, cloud liquid water, water vapor, sea surface winds and sea ice concentration are produced each day on a global basis using all of the SSM/I channel measurements. The SSM/I was developed by the U.S. Navy and first launched on the F-8 DMSP satellite. As a result of a shared processing agreement, all of the SSM/I products are generated by the U.S. Navy and distributed to both the U.S. Air Force and NOAA. The three agencies utilize the products in various ways to improve the analysis and forecast of weather systems.

In addition to flying the SSM/I, the DMSP satellites also carry a temperature sounder (SSM/T) and a water vapor sounder (SSM/T2), both of which were developed by the U.S. Air Force. As shown in Figure 1, the SSM/T was first launched in 1979, and contains seven channels in the 50-60 GHz oxygen band to derive temperature profiles from the surface to about 5 mb. The SSM/T2 is the latest DMSP sensor and was first flown in 1991 aboard the F-12 satellite. It contains window channels at 91 and 150 GHz, and three channels around the strong water vapor line at 183.31 GHz. These channels are used to derive moisture profiles from near the surface to around 300 mb, and to identify precipitation over land and ocean. It is noteworthy that all three instruments (SSM/I, SSM/T, SSM/T2) are currently being flown together aboard the recently launched F-14 satellite, so that radiometric measurements are now available between 19 and 183 GHz. However, the DMSP instruments all have different scan geometry so that even when they are flown together on a single satellite it is very difficult to combine the channel information. To alleviate this problem, a new sensor called the SSM/IS is being developed by the U.S.Air Force to include all of the channels (19-183 GHz) in a single instrument.

As shown in Figure 1, the evolution of microwave radiometers aboard satellites has increased steadily over the past twenty-seven years. Just recently, a modified version of the SSM/I (called TMI) was flown by NASA aboard the TRMM satellite in November 1997; it

contains a 10 GHz channel to improve the estimates of sea surface winds (Wentz et. al., 1986). Of particular importance to NOAA, is the launch in May 1998 of a twenty channel instrument called the Advanced Microwave Sounding Unit (AMSU) which consists of three modules, AMSU-A1, AMSU-A2 and AMSU-B (see Fig. 2 below).

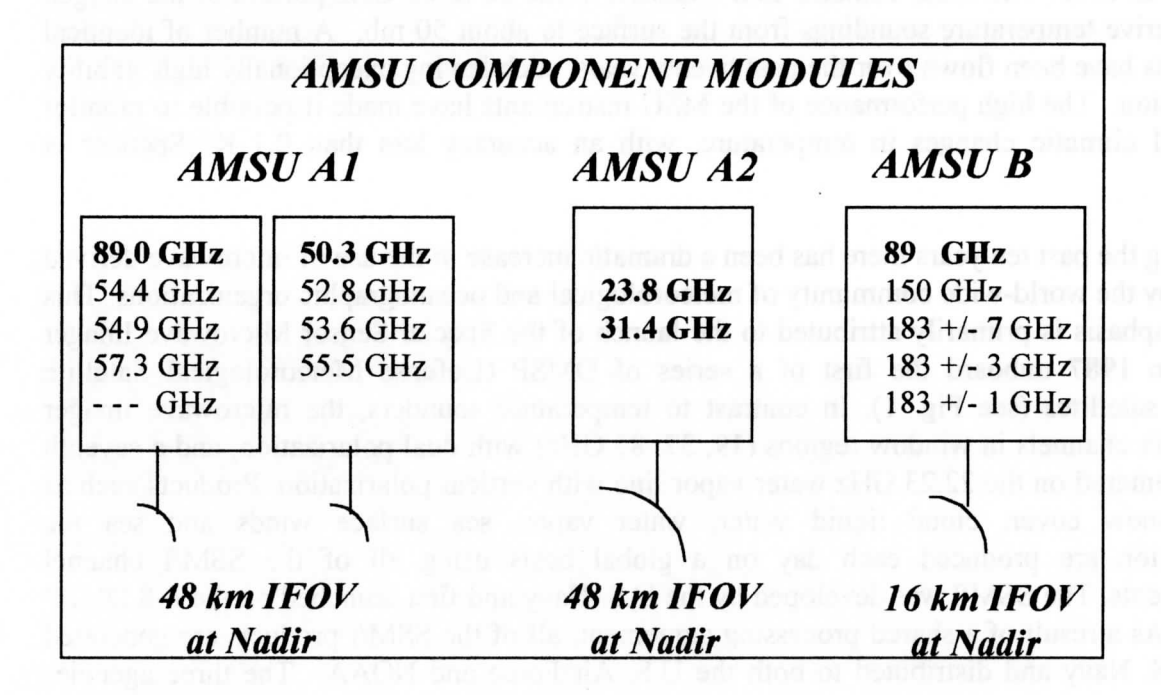


Figure 2. AMSU consists of three separate modules. Window channels used to derive non-sounding products are highlighted.

This long awaited instrument was designed primarily to improve the accuracy of temperature soundings beyond that of the four channel MSU. To obtain this improvement, the AMSU-A1 module includes twelve channels in the 50-60 GHz portion of the oxygen band to provide temperature soundings from the surface to about 1 mb. The AMSU-A1 and A2 modules also includes window channels at 31.4 GHz and 89 GHz to monitor surface features and precipitation, and contains a 23.8 GHz channel for obtaining the total precipitable water over oceans. Figure 2 shows the channels associated with each module, while Table 1 lists the parameters obtained from the window channel measurements along with the estimated accuracy's of each parameter. The AMSU-B module contains four channels around the 183.31 GHz water vapor line for deriving moisture profiles. This paper describes the algorithms for obtaining the so called Day-1 products listed in Table 1. Following one year after launch (Day-2), we will also begin developing the remaining products listed in the Table.

Table 1: AMSU Non-Sounding Products

Ocean Parameters	Channels Used	Parameter Range	Accuracy (rms)	
	Number Recognition	nach (GHz)	Char	
Precipitable water	23, 31 GHz	0 – 70 mm	1.0 mm	
Cloud Liquid Water	23, 31, 50 GHz	0-3 mm	0.05 mm	
Sea Ice Concentration	23, 31 GHz	0 – 100 %	15 %	
Instantaneous Rain Rate	23, 31, 89 GHz	0-30 mm/h	2 mm/h	
Cloud Ice Content *	23, 89, 150 GHz	0 - 1 mm	TBD	
Sea Surface Wind *	23, 31, 50 GHz	0 - 50 m/s	TBD	
	March 19 at No.	0.10 2.54	18.83	
	Par -	051	1 021	
Land Parameters		(83)7	e tradit	
		GIEL	c C*(8)	
Snow Cover	23, 31, 89 GHz	0-100 %,	5 %	
Instantaneous Rain Rate	23, 89, 150 GHz	0 - 30 mm/h	3 mm/h	
Surface Emissivity	23, 31, 50 GHz	0.75 - 0.95	0.02	
Snow Depth *	23, 31, 89 GHz	0 - 30 cm	TBD	
Surface Temperature *	23, 31, 50 GHz	250 – 320 K	TBD	
Surface Wetness *	23, 31, 50 GHz	TBD	TBD	
		and the car	attiction starred but	

DAY-2 Products

2. COMPARISONS BETWEEN AMSU AND DMSP SENSORS

The algorithms developed for AMSU-A are primarily based on knowledge acquired using SSM/I measurements. (Ferraro et., al 1994). Similarly, algorithms developed for AMSU-B are based on SSMT/2 measurements (Grody et al., 1996). For comparison purposes, Table 2 lists the channel frequencies for the SSM/I, SSM/T2 and AMSU instruments. Also listed are the different footprints (i.e., field of view at half power) viewed by each sensor. The SSM/I is a conical scanner so that the footprints are independent of the azmuthal scan angle. The other sensors use a cross-track scanning mechanism so that the footprint can increase by more than a factor of two as the instrument scans from nadir to the limb position. For large scale features such as atmospheric temperature and water vapor, the smoothing due to larger footprints is often minimal. However, when using a cross-track scanner to derive rain rates and cloud liquid water it is generally important to normalize the measurements to a common resolution. Also, when combining or comparing measurements from different sensors, the different resolutions must also be accounted for. The most commonly used approach is to simply average the product derived by various sensors to the footprint of the lowest resolution instrument.

Table 2. Comparison between AMSU and DMSP Channels

Channels (GHz)		Nadir Resolution (km)				
AMSU	SSM/I	SSMT/2	AMSU	SSM/I	SSMT/2	
21.	19.3	W 252 1 1		60	00	
23.8	22.2	mm202 - 0	48 5:	5 -	Rate	
31.4	37.0	1222	48 30			
50-60		1020	48	_11 /12		
89.0 *	85.5	91.0	48 & 16*	15		
150 *		150	16*		60	
183±7 *		183 ± 7	16*		50	
183±3 *		183±3	16*		50	
183±1 *		183±1	16*	1445	50	

Mixed pixels and Aliasing effects

The DMSP instruments use the full antenna aperture to collect the Earth emitted radiation. While this provides the highest resolution for a given antenna size, the footprint size varies in proportion to the wavelength, i.e., the SSM/I footprint decreases from 60 km at 19 GHz to 15 km at 85 GHz. Different resolutions can result in aliasing effects when the channels are combined to derive geophysical parameters. To eliminate aliasing effects, the antenna system for AMSU-A was designed so that all channels have the same instantaneous field of view (IFOV). Similarly the AMSU-B channels all have the same footprint (see Table 2 and Figure 2). As such, the surface emissivity and cloud measurements obtained from the window channels (23.8, 31.4, 50.3 GHz) can be used to correct the lower temperature sounding channels at 52.8 and 53.6 GHz, without having to account for differences in footprint size.

In the case of the SSM/I, aliasing effects result in false identification around coast lines and lake boundaries when the 19 and 85 GHz channels are subtracted to identify snow cover and precipitation. However, even if the aliasing effects are minimized by reducing the resolution of all channels to a common footprint, the false identification around coast lines still exists due to the overlap of the microwave footprint between land and ocean, i.e., mixed pixel effect. Investigators have found that the most efficient means of resolving both of these problems (aliasing and mixed pixel) is to simply eliminate the measurements within a certain distance of water boundaries. This approach has been adopted for both the SSM/I and AMSU instruments. A more physically based, and more complicated approach, would involve the retrieval of surface emissivity from the window channel measurements, and the subsequent correction of the geophysical algorithms using the retrieved emissivity.

3. AMSU ALGORITHMS

From an historical point of view it should be understood that AMSU was designed to obtain vertical profiles of temperature and water vapor. The "non-sounding" products listed in Table 1 (excluding precipitable water) were never envisioned around 1980 when AMSU was designed. While the AMSU contains many of the important frequencies needed to derive the parameters listed in Table 1, it does not contain low frequency window channels (< 23 GHz) or provide polarization information. For example, we have only learned following the launch of the SSM/I in 1987, that polarization information is important for improving the identification and classification of land surfaces. This concluding section briefly overviews the algorithms developed for the Day-1 products listed to in Table 1. Since some of the algorithms (e.g., precipitation and snow cover) can involve numerous steps in a decision tree, the complete procedure is given in the Appendix.

Water vapor and Cloud liquid water

Since the sea surface emissivity can be accurately modeled, radiative transfer simulations have been used to derive algorithms for ocean products such as cloud liquid water, Q, and precipitable water, V. The algorithms (in units of mm) are given as follows;

$$V = \cos \theta \left[C_0 + C_1 \Psi(23.8) + C_2 \Psi(31.4) \right]$$
 (1)

$$Q = \cos \theta \left[D_0 + D_1 \Psi(23.8) + D_2 \Psi(31.4) \right]$$
 (2)

where $\Psi(v) = \ln[285 - T_B(v)]$, and $T_B(v)$ are the AMSU brightness temperature measurements at frequency v. The coefficients C_i and D_i are as follows;

$$C_0 = 2.47.92 - (69.235 - 44.177 \cos \theta) \cos \theta$$
, $C_1 = -116.270$, $C_2 = 73.409$
 $D_0 = 8.240 - (2.622 - 1.846 \cos \theta) \cos \theta$, $D_1 = 0.754$, $D_2 = -2.265$

The scan angle (limb) corrections given in (1) and (2) are functions of $Cos \,\theta$, which is a symmetrical function of θ . However, when applying (2) to the AMSU measurements, one observes consistently more liquid water on one side of nadir than the other side. The asymmetry is most predominant as the antenna beam approaches the Earth's horizon and is a result of two effects. As the scan angle increases from nadir, any left-right asymmetry in the antenna side lobes results in different amounts of cold space radiation (also satellite emitted and reflected radiation) being received on opposite sides of the scan. This effect was first noted from the MSU instrument. It was accounted for using fixed adjustments as a function of beam position and appears to be the main source of asymmetry for the AMSU-A1 module. Asymmetry in the AMSU-A2 channel measurements also results from blockage on one side of the scan by the solar panel onboard the spacecraft. This effect increases the asymmetry beyond that of the AMSU-A1 module, and was not encountered on previous NOAA

satellites. NESDIS personnel are developing corrective procedures for the AMSU-A asymmetry effects.

In order to extend the water vapor and cloud liquid water to high latitudes, the effects of sea ice must be identified and edited out of the data. Sea ice can increase the emissivity to that of land surfaces and result in large overestimates of both water vapor and liquid water. An algorithm for obtaining sea ice concentration has been developed (discussed later), and uses the following discriminate function to identify sea ice,

$$DF1 = 2.85 + 0.020 T_B(23) - 0.028 T_B(50) . (3)$$

This function was obtained using AMSU measurements over high latitude oceans that contained varying amounts of sea ice, clouds and precipitation. As such it should be applied only for latitudes beyond 50 degrees of the equator. Values in excess of 0.0 and 0.2 are found to filter out sea ice for the liquid water and water vapor products, respectively.

Precipitation over Land and Ocean

For precipitating clouds, the instantaneous rain rate depends on the liquid water and descent time of the rain drops, i.e., Rain rate = Q/τ . In actual practice, a rain rate relationship will be obtained by correlating the liquid water measurements of (2) against co-located rain gauge and radar measurements. Liquid water greater than 0.3 mm is generally associated with precipitation while lower values are considered rain-free. This technique of measuring precipitation is referred to as the emission approach since it uses low frequency emission measurements over oceans. A different technique uses the high frequency scattering by ice particles to estimate rain rates. It was originally developed for the SSM/I and SSM/T2 and is very appealing since it is applicable over land as well as oceans. Also, since the scattering technique uses the highest frequency channels, the rain rates are derived at the highest resolution for both the DMSP and AMSU sensors.

The following scattering indices were developed to identify scattering features over land and ocean using AMSU-A channel measurements;

$$SI_{Land} = T_B(23) - T_B(89)$$
 (4a)

$$SI_{Ocean} = -113.2 + [2.41 - 0.0049 T_B(23)] T_B(23) + 0.454 T_B(31) - T_B(89)$$
 (4b)

where SI $_{Land} \ge 3$ and SI $_{Ocean} \ge 9$ are used to identify precipitation. The scattering indices were obtained using scatter-free AMSU data over the corresponding surfaces, and regressing the high frequency channel at 89 GHz against the lower frequency channels. Scattering indices provide a measure of the scattering at high frequencies (e.g., 89 GHz) relative to low frequency channels. In the case of precipitation over land, the index represents the first of many steps (Grody, 1991) needed to identify and discriminate among other scattering features (e.g., snow cover, deserts). The complete decision tree is given in the Appendix.

The AMSU-B channels at 89 and 150 GHz will be used to derive rain rates at the highest resolution (16 km at nadir). Similar channels were included on the SSM/T2, and experimental algorithms were developed to identify precipitation using the following indices,

$$SI_{Land} = [42.72 + 0.85 T_B(91)] - T_B(150)$$
 (5a)

$$SI_{Ocean} = .013\{T_B(91) + 33.58 \ln[300 - T_B(150)] - 341.17\}$$
 (5b)

Over land, the scattering index, SI_{Land} , is an estimate of the scattering effect at 150 GHz relative to the 91 GHz channel. Rain rates exceeding 1 mm/h are identified when the index exceeds a 5 K threshold (Grody et al., 1996). Over oceans the index, SI_{Ocean} , was found to approximate the liquid water measurements obtained from co-located SSM/I data. Also, values of SI_{Ocean} greater than 0.35 mm was found to correlate well with SSM/I observations of precipitation. In order to derive rain rates the indices (4) and (5) must be calibrated against coincident radar and rain gauge measurements in a manner similar to that mentioned previously when discussing the emission technique. Also, at present no corrections have been made to account for the effects of angular scanning and varying footprint size. These effects, however, will be included when deriving rain rates from the AMSU-B channels.

Sea Ice Concentration

The sea ice concentration is obtained by assuming that the field of view contains either new ice or multiyear ice mixed with open water. As such, the fractional amount of sea ice, f, is given by

$$f = \frac{\varepsilon - \varepsilon_{\text{water}}}{\varepsilon_{\text{ice}} - \varepsilon_{\text{water}}}$$
(6)

where ϵ is the measured emissivity at the lowest AMSU frequency (23.8 GHz), ϵ water is the emissivity of open water and ϵ ice is the emissivity of ice. The emissivity of water around 0C is 0.45 and the emissivity of ice varies from about 0.95 for new ice to 0.88 for multiyear ice. Multiyear ice scatters microwave radiation and is identified when $T_B(23) - T_B(31) \ge 5$ K.

Based on radiative transfer simulations over land and ocean that includes non-precipitating clouds, the emissivity at 23.8 GHz is given by

$$\varepsilon = A + B T_B(31) + C T_B(23) + D T_B(50)$$
 (7)

where $A = 1.734 - 0.6236 \cos \theta$, $B = 0.0070 + 0.0025 \cos \theta$, C = -0.00106, D = -0.00909.

The accuracy of (6) depends on the *a-priori* emissivity of sea ice and the estimated emissivity (7). While most clouds produce little error, precipitation increases the brightness temperatures at 23 and 31 GHz and results in overestimates of the emissivity (7) and sea ice concentration. As in the case of water vapor and liquid water the same discriminate function (3) is applied for

latitudes beyond 50 degrees of the equator to filter out precipitation. A discriminate value of 0.45 is found to best filter out precipitation without removing actual sea ice.

Snow Cover

For snow cover (also precipitation), the brightness temperature decreases as the frequency increases. As such, the index given by (4a) is used to identify snow cover under most conditions. However, unlike the low density of scatterers found in precipitation, snow cover contains densely packed ice crystals. The scattering at high frequencies becomes reduced relative to the lower frequencies due metamorphic changes in the crystalline structure as the snow ages. It is therefore important to utilize a lower frequency index to identify metamorphosed snow, i.e.,

$$SI_{31} = T_B(23) - T_B(31)$$
. (8)

The absorption by water vapor is larger at 23 GHz than at 31 GHz, so that the index contains a residual atmospheric contribution. This unfortunately produces a positive index similar to that of snow for flooded land. In order to remove this false signature, the index is only applied when $T_B(89) < 230$. As indicated in the Appendix, (8) is combined with (4a) to observe the full range of snow conditions excluding melting snow. As in the case of precipitation over land, the indices represents the first of many steps (Grody, 1991) needed to identify and discriminate snow cover among other scattering features (e.g., precipitation, deserts). The complete decision tree is given in the Appendix.

4. CONCLUSIONS

The paper begins by summarizing the evolution of satellite microwave radiometry in the United States. At NOAA the operational use of this technology began in 1978 with the production of temperature soundings using the MSU, and has been extended in 1998 to include surface features, clouds, precipitation and water vapor soundings using AMSU. A brief overview is given of the AMSU Day-1 product-algorithms listed in Table 1. These products were not even envisioned around 1980 when AMSU was designed. The algorithms are based on scientific knowledge gained as part of the shared processing agreement between the U.S. Navy, Air Force and NOAA. Validation of the Day-1 products is primarily based on SSM/I comparisons and water vapor obtained from radiosonde data. These comparisons demonstrated the need for improved screening of deserts for the snow cover and precipitation products. Much of the future work will also involve the use of AMSU-B higher frequency channels to improve the estimates of precipitation and cloud parameters, e.g., ice water content. Also, methods shall be developed to combine the products from different sensors (e.g., SSM/I) having different scan geometry and footprint size.

APPENDIX: Complete listing of AMSU algorithms

Discriminate Functions: DF1 = 2.85 + .020 T23 - .028 T50; Used to identify (also remove) sea ice Used to identify (also remove) warm deserts DF2 = 5.10 + .078 T23 - .096 T50; DF3 = 10.2 + .036 T23 - .074 T50: Used to identify (also remove) cold deserts 1. Sea Ice Algorithm (ICE) IF Abs(Latitude) < 50 THEN RETURN IF DF1 < 0.45 THEN ICE =0: RETURN $A = 1.7340 - 0.6236 \cos Z$ B = 0.0070 + 0.0025 CosZC = -0.00106D = -0.00909'Theoretical 23 GHz Surface Emissivity (0.3 - 1) E23 = A + B*T31 + C*T23 + D*T50IF T23 - T31 >= 5 THEN EI=0.88 ELSE EI=0.95 FOV contains Multiyear/Water or New Ice/Water ICE = 100*(E23 - 0.45)/(EI - 0.45)'Sea ice concentration within FOV (0 - 100 %) 2. Water Vapor Algorithm (VAP) IF Abs(Latitude) > 50 AND DF1>0.2 THEN RETURN 'Identify and Remove Sea Ice $A = 247.92 - (69.235 - 44.177 \cos Z) \cos Z$ B = -116.270C = 73.409VAP = A + B*Log(285 - T23) + C*Log(285 - T31)VAP = VAP CosZTheoretical Total Precipitable Water (0 - 70 mm) 3. Cloud Liquid Water Algorithm (LIQ) IF Abs(Latitude) > 50 AND DF1>0.0 THEN RETURN 'Identify and Remove Sea Ice $A = 8.240 - (2.622 - 1.846 \cos Z) \cos Z$ B = .0.754C = -2.265LIQ = A + B*Log(285 - T23) + C*Log(285 - T31)LIQ = LIQ CosZ'Theoretical Cloud Liquid Water (0 - 3 mm) 4. Rain Identification (0=No Rain 1=Rain) LAND: TT = 168 + 0.49 T89SIL = T23 - T89IF SIL>= 3 THEN RAIN=1 **ELSE** RAIN=0 IF T23 =< 261 AND T23 < TT THEN RAIN=0 'Remove Snow Cover IF T89 > 273 OR **DF2** < 0.6 THEN 'Remove Warm Deserts RAIN=0 OCEAN: IF Latitude > 50 AND DF1 > 0.0 THEN RETURN 'Identify and Remove Sea Ice $A = 8.240 - (2.622 - 1.846 \cos Z) \cos Z$ B = 0.754C = -2.265LIQ = A + B*Log(285 - T23) + C*Log(285 - T31)'Cloud Liquid Water (0 - 3 mm) LIQ = LIQ CosZSIW = -113.2 + (2.41 - .0049*T23)*T23 + .454*T31 - T89IF LIQ > 0.3 OR SIW > 9 THEN RAIN = 1 ELSE RAIN = 0

'Remove non-precipitating clouds

5. Snow Cover and Glacial Ice (0=No Snow 1=Snow 2=Glacial Ice)

TT = 168 + 0.49 T89SCAT = T23 - T89

SC31 = T23 - T31

IF T89 < 230 AND SCAT< SC31 THEN SCAT = SC31

IF SCAT < 1 AND T23 < 220 THEN SNOW = 2

IF SCAT >= 1 THEN SNOW=1 ELSE SNOW = 0

IF $T23 \ge 262$ OR $T23 \ge TT$ THEN SNOW = 0

IF **DF3** =< 0.35 THEN SNOW=0

Remove Wet Surface effect on SC31 'Identify Glacial Ice

'Remove Precipitation

'Remove some Cold Deserts

REFERENCES

Ferraro, R, N. Grody, D. Forsyth, R. Carey, A. Basist, J. Janowiak, F. Weng, G. Marks and R. Yanamandra, "Microwave Measurements Produce Global Climatic, Hydrologic Data," EOS *Trans.*, American Geophys. Union, 75, 337-343, 1994.

Grody, N.C., 1991: Classification of snowcover and precipitation using the special sensor microwave imager. J. Geophys. Res., 96, 7423-7435.

Grody, N., F. Weng and R. Ferraro, 1996: Comparison between SSM/I, SSM/T2 and radar measurements over the United States, AMS Conference on Satellite Meteorology, Atlanta Ga, 243-247.

Spencer, R., J. Christy and N. Grody, 1990: Global atmospheric temperature monitoring with satellite microwave measurements: Method and results 1979-1984, 3, 1111-1128.

Weng, F., and N. Grody, 1994: Retrieval of cloud liquid water using the Special Sensor Microwave Imager (SSM/I), J. Geophys. Res., 99, 25535-25551.

Wentz, F., L. Mattox and S. Peteherych, 1986: New algorithms for microwave measurements of ocean winds applications to SEASAT and the Special SensorMicrowave Imager, J. Geophys. Res., 91, 2289-2307.

TECHNICAL PROCEEDINGS OF THE TENTH INTERNATIONAL ATOVS STUDY CONFERENCE

Boulder, Colorado 27 January - 2 February 1999

Edited by

J. Le Marshall and J.D. Jasper
Bureau of Meteorology Research Centre, Melbourne, Australia

Published by

Bureau of Meteorology Research Centre PO Box 1289K, GPO Melbourne, Vic., 3001, Australia